

---

# Network insensitivity to parameter noise via adversarial regularization

---

<b>Julian Büchel*</b> SynSense Zürich, Switzerland julian.buchel@synsense.ai	<b>Fynn Faber</b> Dept. of Computer Science ETH Zürich Zürich, Switzerland faberf@ethz.ch	<b>Dylan R. Muir</b> SynSense Zürich, Switzerland dylan.muir@synsense.ai
---	---	---

## Abstract

Neuromorphic neural network processors, in the form of compute-in-memory crossbar arrays of memristors, or in the form of subthreshold analog and mixed-signal ASICs, promise enormous advantages in compute density and energy efficiency for NN-based ML tasks. However, these technologies are prone to computational non-idealities, due to process variation and intrinsic device physics. This degrades the task performance of networks deployed to the processor, by introducing parameter noise into the deployed model. While it is possible to calibrate each device, or train networks individually for each processor, these approaches are expensive and impractical for commercial deployment. Alternative methods are therefore needed to train networks that are inherently robust against parameter variation, as a consequence of network architecture and parameters. We present a new adversarial network optimisation algorithm that attacks network parameters during training, and promotes robust performance during inference in the face of parameter variation. Our approach introduces a regularization term penalising the susceptibility of a network to weight perturbation. We compare against previous approaches for producing parameter insensitivity such as dropout, weight smoothing and introducing parameter noise during training. We show that our approach produces models that are more robust to targeted parameter variation, and equally robust to random parameter variation. Our approach finds minima in flatter locations in the weight-loss landscape compared with other approaches, highlighting that the networks found by our technique are less sensitive to parameter perturbation. Our work provides an approach to deploy neural network architectures to inference devices that suffer from computational non-idealities, with minimal loss of performance. This method will enable deployment at scale to novel energy-efficient computational substrates, promoting cheaper and more prevalent edge inference.

## 1 Introduction

There is increasing interest in NN and ML inference on IoT and embedded devices, which imposes energy constraints due to small battery capacity and untethered operation. Existing edge inference solutions based on CPUs or vector processing engines such as GPUs or TPUs are improving in energy efficiency, but still entail considerable energy cost [1]. Alternative compute architectures such as memristor crossbar arrays and mixed-signal event-driven neural network accelerators promise significantly reduced energy consumption for edge inference tasks. Novel non-volatile memory technologies such as resistive RAM and phase-change materials [2, 3] promise increased memory density with multiple bits per memory cell, as well as compact compute-in-memory for NN inference tasks [4]. Analog implementations of neurons and synapses, coupled with asynchronous digital

routing fabrics, permit high sparsity in both network architecture and activity, thereby reducing energy costs associated with computation.

However, both of these novel compute fabrics introduce complexity in the form of computational non-idealities, which do not exist for pure synchronous digital solutions. Some novel memory technologies support several bits per memory cell, but with uncertainty about the precise value stored on each cycle [5, 6]. Others exhibit significant drift in stored states [7]. Inference processors based on analog and mixed-signal devices [8–11] exhibit parameter variation across the surface of a chip, and between chips, due to manufacturing process non-idealities. Collectively these processes known as “device mismatch” manifest as parameter noise in weights and neuron parameters.

In all cases the mismatch between configured and implemented network parameters degrades the task performance by modifying the resulting mapping between input and output. Existing solutions for deploying networks to inference devices that exhibit mismatch mostly focus on per-device calibration or re-training [12–14]. However, this approach entails significant per-device handling costs, limiting its effectiveness for commercial deployment.

We consider a network to be “robust” if the output of a network to a given input does not change in the face of parameter perturbation. With this goal, network architectures that are intrinsically robust against device mismatch can be investigated [15, 16]. Another approach is to introduce parameter perturbations during training that promote robustness during inference, for example via random pruning (dropout) [17] or by injecting noise [7, 18].

In this paper we introduce a novel solution, by applying adversarial training approaches to parameter mismatch. Most existing adversarial training methods attack the input space. Here we describe an adversarial attack during training that seeks the parameter perturbation that causes the maximum degradation in network response. In summary, we make the following contributions:

- We propose a novel algorithm for gradient-based supervised training of networks that are robust against parameter mismatch, by performing adversarial training in the weight space.
- We demonstrate that our algorithm flattens the weight-loss landscape and therefore leads to models that are inherently more robust to parameter noise.
- We show that our approach outperforms existing methods in terms of robustness.

## 2 Related Work

Research to date has focused mainly on adversarial attacks in the input space. With an increasing number of adversarial attacks, an increasing number of schemes defending against those attacks have been proposed [19–22]. In contrast, adversarial attacks in parameter space have received little attention. Where parameter-space adversaries have been examined, it has been to enhance performance in semi-supervised learning [23] or to improve robustness to *input-space* adversarial attacks [24].

We define “robustness” to mean that the network output should change only minimally in the face of a parameter perturbation — in other words, the weight-loss landscape should be as flat as possible at a loss minimum. Other algorithms that promote flat loss landscapes may therefore also be useful to promote robustness to parameter perturbations.

**Dropout** [17] is a widely used method to reduce overfitting. During training, a random subset of units are chosen with some probability, and these units are pruned from the network for a single trial or batch. This results in the network learning to distribute its computation across many units, and acts as a regularization against overfitting.

**Entropy-SGD** [25] is a network optimisation method that minimises the local entropy around a solution in parameter space. This results in a smoothed parameter-loss landscape that should penalize sharp minima.

**Adversarial Block Coordinate Descent (ABCD)** [23] was proposed in order to complement input-space smoothing with weight-space smoothing in semi-supervised learning. ABCD repeatedly picks half of the network weights and performs one step of gradient ascent on them, followed by applying gradient descent on the other half.

**Adversarial Weight Perturbation (AWP)** [24] was designed to improve the robustness of a network to adversarial attacks in the input space. The authors use Projected Gradient Ascent (PGA) on the network parameters to approximate a worst case perturbation of the weights  $\Theta'$ . Having identified an adversarial perturbation in the weight-space, an adversarial perturbation in the input-space is also found using PGA. Finally, the original weights  $\Theta$  are updated using the gradient of the loss evaluated at the adversarial perturbation  $\Theta'$ .

**TRadeoff-inspired Adversarial DEfense via Surrogate-loss minimization (TRADES)** [20] is a method for training networks that are robust against adversarial examples in the input space. The method consists of adding a boundary loss term to the loss function that measures how the network performance changes when the input is attacked. The boundary loss does not take the labels into account, so scaling it by a factor  $\beta$  allows for a principled trade-off between the robustness and the accuracy of the network.

**Noise injection during the forward pass** [18] is a simple method for increasing network robustness to parameter noise. This method adds Gaussian noise to the network parameters during the forward pass and computes weight gradients with respect to the original parameters. This method regularizes the gradient magnitudes of output units with respect to the weights, thus enforcing distributed information processing and insensitivity to parameter noise. We refer to this method as “Forward Noise”.

### 3 Methods

Code to replicate our methods as well as all experiments described in this paper is provided at [https://gitlab.com/synsense/buchel2021\\_adversarial\\_training](https://gitlab.com/synsense/buchel2021_adversarial_training).

We use  $\Theta$  to denote the set of parameters of a neural network  $f(x, \Theta)$  that are trainable and susceptible to mismatch. The adversarial weights are denoted  $\Theta^*$ , where  $\Theta_t^*$  are the adversarial weights at the  $t$ -th iteration of PGA. We denote the PGA-adversary as a function  $\mathcal{A}$  that maps parameters  $\Theta$  to attacking parameters  $\Theta^*$ . We denote a mini-batch of training examples as  $X$  with  $y$  being the corresponding ground-truth labels.  $\prod_{\mathcal{E}_\zeta^p}(m)$  denotes the projection operator on the  $\zeta$ -ellipsoid in  $l^p$  space. The operator  $\odot$  denotes elementwise multiplication.

As shown in [7], the effect of component mismatch on a network parameter can be modelled using a Gaussian distribution where the standard deviation depends linearly on the parameter magnitude. For complex Spiking Neural Networks (SNNs), “network parameters” can refer to additional quantities such as neuronal and synaptic time constants or spiking thresholds. Our training approach can be equally applied to these additional parameters. However, in this paper we restrict ourselves to perturbations in the network weights for simplicity.

We define the value of an individual parameter when deployed on a neuromorphic chip as

$$\Theta^{\text{mismatch}} \sim \mathcal{N}(\Theta, \text{diag}(\zeta|\Theta|)) \quad (1)$$

where  $\zeta$  governs the perturbation magnitude, referred to as the “mismatch level”. The physics underlying the neuronal- and synaptic circuits lead to a model where the amount of noise introduced into the system depends linearly on the magnitude of the parameters. If mismatch-induced perturbations had constant standard deviation independent of weight values, one could use the weight-scale invariance of neural networks as a means to achieve robustness, by simply scaling up all network weights (See Fig. S3). The linear dependence of weight magnitude and mismatch noise precludes this approach.

In contrast to adversarial attacks in the *input space* [21, 26–28], our method relies on adversarial attacks in *parameter space*. During training, we approximate the worst case perturbation of the network parameters using PGA and update the network parameters in order to mitigate these attacks. To trade-off robustness and performance, we use a surrogate loss [20] to capture the difference in output between the normal and attacked network. Algorithm 1 illustrates the training procedure in more detail.

Unlike adversarial training in the input space, where adversarial inputs can be seen as a form of data augmentation, adversarial training in the parameter space poses the following challenge: Because the parameters that are attacked are the same parameters being optimized, performing gradient descent using the same loss that was used for PGA would simply revert the previous updates and no learning would occur. ABCD circumvents this problem by masking one half of the parameters

```

begin
   $\Theta_0^* \leftarrow \Theta + |\Theta| \epsilon \odot R ; R \sim \mathcal{N}(0, 1)$ 
  for  $t = 1$  to  $N_{steps}$  do
     $g \leftarrow \nabla_{\Theta_{t-1}^*} \mathcal{L}_{Rob}(f(\Theta, X), f(\Theta_{t-1}^*, X))$ 
     $v \leftarrow \arg \max_{v: \|v\|_p \leq 1} v^T g$ 
     $\Theta_t^* \leftarrow \prod_{\mathcal{E}_\zeta^p}(\Theta_{t-1}^* + \alpha \odot v)$ 
  end
   $\Theta \leftarrow \Theta - \eta \nabla_{\Theta} \mathcal{L}_{Nat}((\Theta, X), y) + \beta \mathcal{L}_{Rob}(\Theta, \Theta_{N_{steps}}^*, X)$ 
end

```

**Algorithm 1:** In  $l_\infty$ ,  $v$  corresponds to  $\text{sign}(g)$  and the step size  $\alpha$  is  $\frac{|\Theta| \odot \zeta}{N_{steps}}$ .  $\prod_{\mathcal{E}_\zeta^p}(m)$  denotes the projection operator on the  $\zeta$ -ellipsoid in  $l^p$  space. In  $l^\infty$  this corresponds to  $\min(\max(m, \Theta - \epsilon), \Theta + \epsilon)$  with  $\epsilon = \zeta \odot |\Theta|$ .

in the adversarial loop and masking the other half during the gradient descent step. However, this limits the adversary in its power, and requires multiple iterations to be performed in order to update all parameters at least once. AWP approached this problem by assuming that the gradient of the loss with respect to the attacking parameters can be used in order to update the original parameters to favor minima in flatter locations in weight-space. However, it is not clear whether this assumption always holds since the gradient of the loss with respect to the attacking parameters is not necessarily the same direction that would lead to a flatter region in the weight loss-landscape.

We approach this problem slightly differently: Similar to the TRADES algorithm [20], our algorithm optimizes a natural (task) loss and a separate robustness loss.

$$\mathcal{L}_{Gen}(\Theta, X, y) = \mathcal{L}_{Nat}(\Theta, X, y) + \beta \mathcal{L}_{Rob}(\Theta, \mathcal{A}(\Theta), X)$$

Using a different loss for capturing the susceptibility of the network to adversarial attacks enables us to simultaneously optimise for performance and robustness, without PGA interfering with the gradient descent step. In our experiments,  $\mathcal{L}_{Rob}$  is defined as

$$\mathcal{L}_{Rob}(\Theta, \mathcal{A}(\Theta), X) = \text{KL}(f(\Theta, X), f(\Theta^*, X)) \quad (2)$$

This formulation comes with a large computational overhead since it requires computing the Jacobian  $\mathbf{J}_{\Theta^*}(\Theta)$  of a complex recurrent relation between  $\Theta$  and  $\Theta^*$ . To make our algorithm more efficient we assume that the Jacobian is diagonal, meaning that  $\Theta^* = \Theta + \Delta\Theta$  for some  $\Delta\Theta$  given by the adversary. In  $l_\infty$ , the Jacobian can then be calculated efficiently using (see suppl. material for details):

$$\mathbf{J}_{\Theta^*}(\Theta) = \mathbf{I} + \text{diag} \left[ \frac{\text{sign}(\Theta) \odot (\zeta + \epsilon \cdot R_1)}{N_{steps}} \odot \sum_{t=1}^{N_{steps}} \text{sign}(\nabla_{\Theta_t^*} \mathcal{L}_{Rob}(f(\Theta, X), f(\Theta_t^*, X))) \right]$$

By making this assumption, our algorithm effectively multiplies the original training time by the number of PGA steps, similar to [23, 24].

Because component mismatch effects each parameter independently and is proportional to the magnitude of each parameter, one has to model the space in which the adversary can search for a perturbation using an axis-aligned ellipsoid in  $l_2$  and an axis-aligned box in  $l_\infty$ . Using an  $\epsilon$ -ball where the radius depends linearly on the individual parameter sets [23, 24, 29] would either give the adversary too little or too much attack space. Projecting onto an axis-aligned ellipsoid in  $l_2$  corresponds to solving the following optimization problem [30, 31], which does not have a closed-form solution:

$$\begin{aligned}
 x^* &= \arg \min_x \frac{1}{2} \|m - x\|_2 \\
 \text{s.t. } &(x - c)^T W^{-2} (x - c) \leq 1
 \end{aligned}$$

where  $W = \text{diag}(|\Theta| \odot \zeta) + \mathbf{I} \cdot \zeta_{\text{const}}$ ,  $c = \Theta$  and  $m = \Theta^* + \alpha \odot v$ . Because of the computational overhead this would incur, we only consider the  $l_\infty$  case in our experiments.

## 4 Results

The ultra-low power consumption of mixed-signal neuromorphic chips make them suitable for edge-applications, such as always-on voice detection [32], vibration monitoring [33] or always-

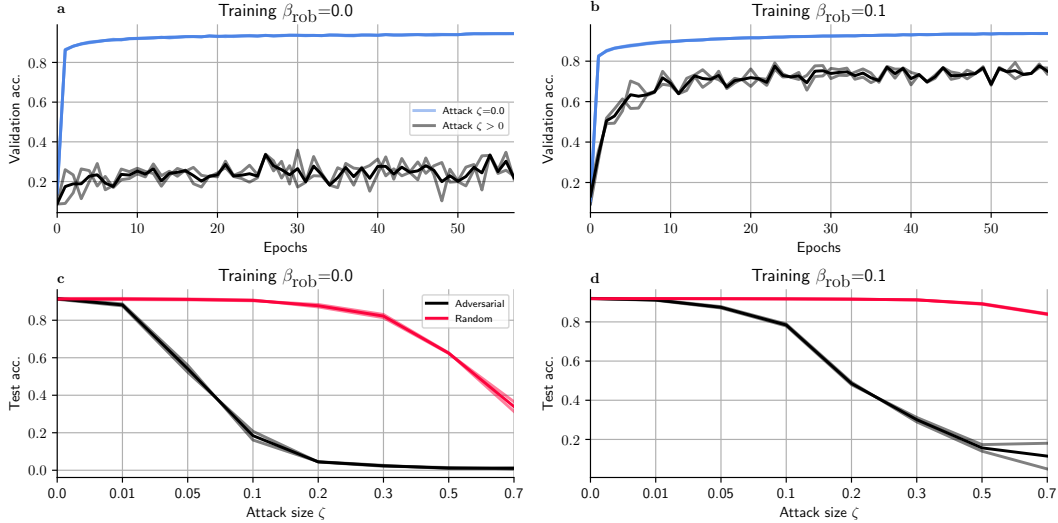


Figure 1: **Our adversarial attack is effective at decreasing the performance of a network, and using our attack during training protects a network from disruption.** (a) A network trained using standard gradient descent (i.e.  $\beta_{\text{rob}} = 0.0$ ) on the F-MNIST task is disrupted badly by the adversary during inference ( $\zeta = 0.1$ ; black curve). (b) When the same network is trained with adversarial attacks ( $\beta_{\text{rob}} = 0.1$ ) during training, the network is protected from adversarial attacks (high accuracy of attacked network; black curve). (c) When no adversarial training is performed ( $\beta_{\text{rob}} = 0.0$ ), random noise (red) and adversarial attacks (black) both disrupt network performance for increasing attack size  $\zeta$ . (d) When adversarial training is performed ( $\beta_{\text{rob}} = 0.1$ ), the network is significantly protected against random and adversarial weight perturbations.

on face recognition [34]. For this reason, we consider two compact network architectures in our experiments: A Spiking Recurrent Neural Network (SRNN) with roughly 65k trainable parameters and a conventional CNN with roughly 500k trainable parameters (see S1 for more information). We trained these models to perform three different tasks:

- Speech command detection of 6 classes [35];
- ECG-anomaly detection on 4 classes [13]; and
- Fashion-MNIST (F-MNIST): clothing-image classification on 10 classes [36].

We compared several training and attack methods, beginning with a standard gradient-descent approach using the Adam optimizer [37] (“Standard”). Learning rate varied by architecture, but was kept constant when comparing training methods on an architecture. We examined networks trained with dropout [17], AWP [24], ABCD [23], and Entropy-SGD [25]. The adversarial perturbations used in AWP and ABCD were adapted to our mismatch model (i.e. magnitude-dependent in  $l_\infty$ ). We further adapted AWP so that the input data is never attacked.

Unless stated otherwise, a dropout probability of 0.3 was used in the dropout models; the regularization parameter  $\beta_{\text{Rob}}$  in our method was set to 0.25 and  $\gamma$  in AWP was set to 0.1. When Gaussian noise was applied to the weights during the forward pass [18] a standard deviation of 0.3 was used. For Entropy-SGD, we set the number of inner iterations to 10 with a Langevin learning rate of 0.1. Because Entropy-SGD and ABCD have inner loops, the number of total epochs were reduced accordingly. All other models were trained for the same number of epochs (no early stopping) and the model with the highest validation accuracy was selected.

We trained 168 models in parallel on a CPU cluster, with each model requiring on average 12 hours of compute time on a single CPU with 16 cores and 32Gb RAM.

**Effectiveness of adversarial weight attack** We examined the strength of our adversarial weight attack during inference and training. Standard networks trained using gradient descent alone with no

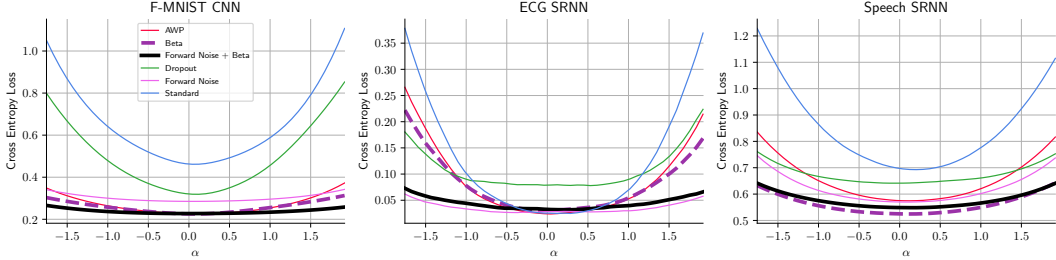


Figure 2: **Our training method flattens the weight-loss landscape.** When moving away from the trained weight minimum ( $\alpha = 0$ ) in randomly-chosen directions, we find that our adversarial training method (Beta; Beta+Forward) finds deeper minima (for F-MNIST and Speech tasks) at flatter locations in the cross-entropy loss landscape. See text for further details.

additional regularization (Fig. 1a, “Standard”) were disrupted badly by our adversarial attack during inference ( $\zeta = 0.1$ ; final mean test accuracy  $91.40\% \rightarrow 17.50\%$ ), and this was not ameliorated by further training. When our adversarial attack was implemented during training (Fig. 1a,  $\beta_{\text{rob}} = 0.1$ ), the trained network was protected from disruption both during training and during inference (final test accuracy  $91.97\% \rightarrow 78.41\%$ ).

Our adversarial attack degrades network performance significantly more than a random perturbation. Because our adversary uses PGA during the attack, it approximates a worst-case perturbation of the network within an ellipsoid around the nominal weights  $\Theta$ . We compared the effect of our attack against a random weight perturbation of equal magnitude. For increasing perturbation size during inference (Fig. 1c;  $\zeta$ ), our adversarial attack disrupted the performance of the standard network significantly more than a random perturbation (test acc.  $91.40\% \rightarrow 17.50\%$  (attack) vs.  $91.40\% \rightarrow 90.63\%$  (random) for  $\zeta = 0.1$ ). When our adversarial attack was applied during training (Fig. 1d;  $\beta_{\text{rob}} = 0.1$ ), the network was protected against both random and adversarial attacks for magnitudes up to  $\zeta = 0.7$  and  $\zeta = 0.1$ , respectively.

**Flatness of the weight-loss landscape** Under our definition of robustness, the network output should change only minimally when the network parameters are perturbed. This corresponds to a loss surface that is close to flat in weight space. We measured the weight-loss landscape for trained networks, compared over alternative training methods and for several architectures (Fig. 2). We examined only cross-entropy loss (i.e. task loss) over the test set, and not the adversarial attack loss component (KL divergence loss; see Eq. 2). For each trained network, we chose a random vector  $v \sim \mathcal{N}(\mathbf{0}, \zeta|\Theta|)$  and calculated  $\mathcal{L}_{\text{Nat}}(f(X_{\text{test}}, \Theta + \alpha \cdot v), y_{\text{test}})$  for many evenly-spaced  $\alpha \in [-2, 2]$ . This process was repeated 5 times for  $\zeta = 0.2$ , and the means plotted in Fig. 2. Weight-loss landscapes for the individual trials are shown in Fig. S1.

Our adversarial training approach found minima of trained parameters  $\Theta$  in flatter areas of the weight-loss landscape, compared with all other approaches examined (flatter curves in Fig. 2). In most cases our training approach also found deeper minima at lower  $\mathcal{L}_{\text{cce}}$ , reflecting better task performance. These results are reflected in the better generalization performance of our approach (see Table 1). Not surprisingly, dropout and AWP also lead to flatter minima than the Standard network with no regularization. ABCD and Entropy-SGD were not included in Fig. 2 because they did not outperform the Standard model.

**Network robustness against parameter mismatch** We evaluated the ability of our training method to protect against simulated device mismatch. We introduced frozen parameter noise into models trained with adversarial attack, with noise modelled on that observed in neuromorphic processors [7, 16]. In these devices, uncertainty associated with each weight parameter is approximately normally distributed around the nominal value, with a standard deviation that scales with the weight magnitude (Eq 1). We measured test accuracy under simulated random mismatch for 100 samples across two model instances. A comparison of our method against standard training is shown in Fig. 3. For mismatch levels up to 70% ( $\zeta = 0.7$ ), our approach protected significantly against

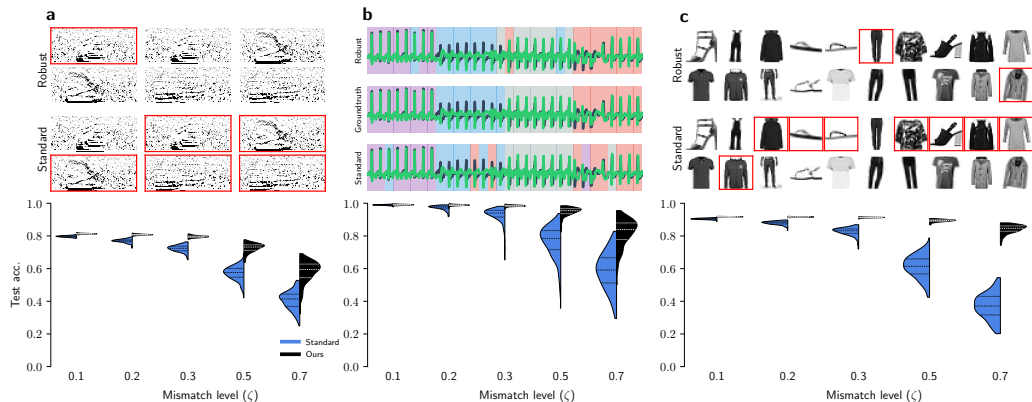


Figure 3: **Adversarial attack during training protects networks against mismatch-induced parameter noise.** Networks were evaluated for the Speech (a), ECG (b) and F-MNIST tasks (c), under increasing levels of simulated mismatch ( $\zeta$ ). Networks trained using standard gradient descent (“Standard”) were disrupted by mismatch levels  $\zeta > 0.1$ . At all mismatch levels our adversarial training approach performed significantly better in the presence of mismatch (higher test accuracy).

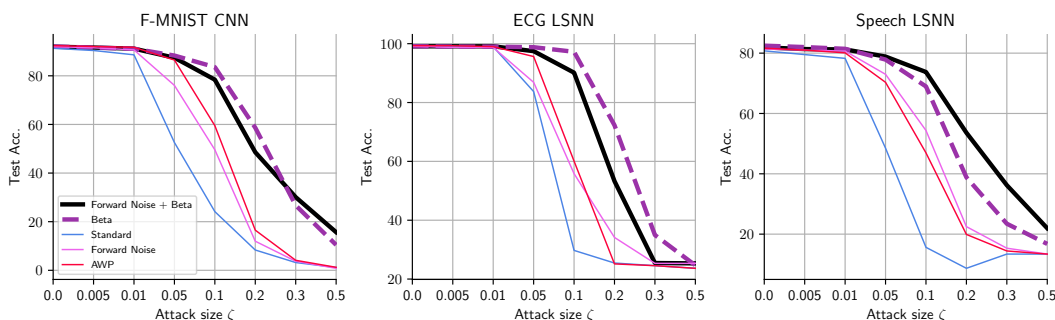


Figure 4: **Our training method protects against task-adversarial attacks in parameter space.** Networks trained under several methods were attacked using a PGA adversary that directly attacked the task performance  $\mathcal{L}_{cce}$ . Our adversarial training approach (bold; dashed) outperformed all other methods against this attack.

simulated mismatch for all three tasks examined ( $p < 2 \times 10^{-8}$  in all cases; U test). A more detailed comparison between the different models is given in Table 1.

**Network robustness against direct adversarial attack on task performance** Our training approach improves network robustness against mismatch parameter noise. We further evaluated the robustness of our trained networks against a parameter adversary that directly attacks task performance, by performing PGA on the cross-entropy loss  $\mathcal{L}_{Nat}$ . Note that this is separate from the adversary used in our training method, which attacks the boundary loss (Eq.2). The AWP method uses the cross-entropy loss to find adversarial parameters during training. Nevertheless, we found that our method consistently outperforms all other compared methods for increasing attack magnitude  $\zeta$  (Fig. 4). In networks trained with our method, the adversary needed to perform a considerably larger attack to significantly reduce performance (test accuracy  $< 70\%$ ). ABCD and Entropy-SGD were not included in the comparison because they did not outperform the standard network.

**Provable robustness for SRNNs** We investigated the provable robustness of SRNNs trained using our method using abstract interpretation [38–40]. In this analysis a function  $f(x, \Theta)$  (in our case, a neural network with input  $x$  and parameters  $\Theta$ ) is overapproximated using an *abstract domain*. We

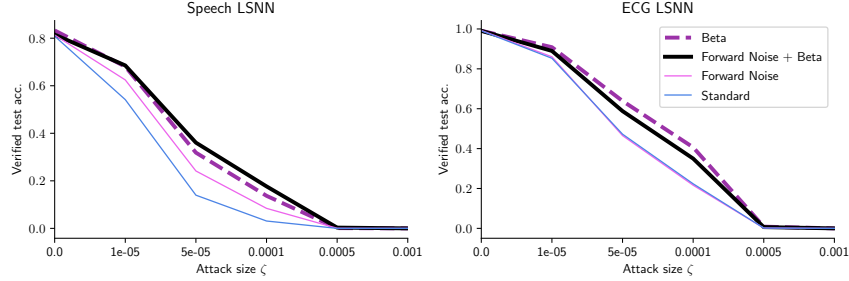


Figure 5: **Networks trained with our method are provably more robust than those trained with standard gradient descent or forward noise alone.** We used interval bound propagation to determine the proportion of test samples that are verifiably correctly classified, under increasing weight perturbations  $\zeta$ . For both the Speech and ECG tasks, computed on the trained SRNNs, our method was provably more robust for  $\zeta < 5 \times 10^{-4}$ .

specify the weights  $\Theta$  in our network as an interval parameterised by the attack size  $\zeta$ , spanning  $[\Theta - \zeta|\Theta|, \Theta + \zeta|\Theta|]$ . Computations through the network are performed on these intervals rather than on discrete values. By propagating the intervals through a network over a test set, we obtain output logits that are also expressed as intervals. The final classification of the network is made using an argmax operator. For provability of network performance, we consider that a test sample  $x$  is correctly classified when the lower bound of the logit interval for the correct class is the maximum lower bound across all logit intervals, and when the logit interval for the correct class is disjoint from the other logit intervals. When the logit interval for the correct class overlaps with another logit interval, that test sample is not considered to be provably correctly classified.

We examined the proportion of provably correctly classified test samples for the Speech and ECG tasks, under a range of attack sizes  $\zeta$ , and comparing our approach against standard gradient descent and against training with forward-pass noise only (Fig. 5). We found that our approach is provably more correct over increasing attack size  $\zeta$  (higher verified test accuracy). Note that interval domain analysis provides a relatively loose bound [39], with the implication that the results here probably underestimate the true performance of our method.

## 5 Discussion

We proposed a new training approach that includes adversarial attacks on the parameter space during training. Our attack disrupts the behaviour of a network by seeking a small weight perturbation that causes a maximal change in network output, by iteratively applying PGA. During training we jointly optimize a natural- and a robustness loss, where the robustness loss captures the susceptibility of the network to the adversarial attack. We evaluated our method on three tasks (F-MNIST; Speech-commands and ECG analysis), and measured the robustness of our approach against several forms of weight-space perturbation during inference. We compared our approach against several other training methods that could be expected to provide robustness against parameter perturbations.

Our proposed adversarial attack was significantly stronger than random weight perturbations at disrupting the performance of a trained network. Including the adversarial attack during training significantly protected the trained network from weight perturbations during inference. Our approach found minima in the weight-loss landscape that usually corresponded to lower loss values, and were always in flatter regions of the loss landscape. This indicates that our approach found network solutions that are less sensitive to parameter variation, and therefore more robust. Our approach was more robust than several other methods for inducing robustness and good generalisation.

To the best of our knowledge, our work represents the first example of interval bound propagation applied to SNNs, and the first application of parameter-space adversarial attacks to promote network robustness against device mismatch for mixed-signal compute.

**Limitations** Our experiments only considered the impact of weight perturbations, and did not examine the influence of uncertainty in other parameters of mixed-signal neuromorphic processors such as time constants or spiking thresholds. Our approach can be adapted to include adversarial

Table 1: **Results of training multiple networks using several methods over three tasks.** Networks were evaluated under different levels of mismatch ( $\zeta$ ). The highest performance in each row is in **bold**.

CNN																		
Mismatch	Forward Noise + Beta 0.1			Beta 0.25			Standard			Forward Noise			AWP			Dropout = 0.3		
	Mean Acc.	Std.	Min.	Mean Acc.	Std.	Min.	Mean Acc.	Std.	Min.	Mean Acc.	Std.	Min.	Mean Acc.	Std.	Min.	Mean Acc.	Std.	Min.
0.0	91.88	<b>0.00</b>	91.88	92.11	0.22	91.89	91.30	0.15	91.15	92.00	0.02	91.98	92.35	0.12	<b>92.23</b>	<b>92.42</b>	0.24	92.18
0.1	91.77	0.12	91.29	91.59	0.26	90.91	90.45	0.37	88.80	91.94	<b>0.09</b>	91.69	<b>92.19</b>	0.16	<b>91.78</b>	91.13	0.85	86.50
0.2	91.62	<b>0.16</b>	<b>91.19</b>	90.67	0.42	89.28	87.93	1.03	83.40	<b>91.63</b>	<b>0.16</b>	91.06	91.42	0.44	89.87	88.71	1.55	80.97
0.3	<b>91.25</b>	<b>0.22</b>	<b>90.36</b>	89.64	0.65	87.10	82.70	2.45	71.99	91.01	0.26	90.01	89.88	0.95	85.11	84.94	3.06	72.97
0.5	<b>89.36</b>	<b>0.73</b>	<b>86.84</b>	85.96	1.87	76.28	61.14	6.92	42.46	87.82	0.88	84.37	82.59	3.66	66.73	71.74	5.84	53.10
0.7	<b>84.19</b>	<b>2.63</b>	<b>74.25</b>	79.39	4.40	59.15	36.93	7.73	20.17	78.48	2.95	69.67	65.38	8.27	40.66	53.91	9.03	22.49
ECG LSNN																		
Mismatch	Forward Noise + Beta 0.1			Beta 0.25			Standard			Forward Noise			AWP			Dropout = 0.3		
	Mean Acc.	Std.	Min.	Mean Acc.	Std.	Min.	Mean Acc.	Std.	Min.	Mean Acc.	Std.	Min.	Mean Acc.	Std.	Min.	Mean Acc.	Std.	Min.
0.0	99.07	0.34	98.73	99.10	0.07	<b>99.03</b>	99.07	<b>0.04</b>	<b>99.03</b>	<b>99.25</b>	0.37	98.88	99.22	0.19	<b>99.03</b>	98.10	0.11	97.99
0.1	99.04	0.27	98.36	98.96	0.24	98.28	98.95	0.27	97.76	<b>99.09</b>	<b>0.19</b>	<b>98.66</b>	98.93	0.31	97.69	97.71	0.34	96.72
0.2	98.87	0.35	96.94	98.16	0.71	93.96	97.22	1.46	91.87	<b>99.01</b>	<b>0.26</b>	<b>98.06</b>	97.71	0.97	93.06	96.89	0.87	93.81
0.3	98.45	<b>0.45</b>	<b>96.49</b>	96.34	1.95	89.33	92.97	4.38	65.30	<b>98.59</b>	0.52	95.30	94.60	2.93	81.34	94.85	2.47	85.60
0.5	<b>94.86</b>	<b>2.69</b>	82.39	86.22	6.66	60.75	76.55	9.61	35.75	94.44	2.86	<b>82.84</b>	80.32	8.08	41.94	87.56	6.05	64.10
0.7	<b>82.02</b>	<b>8.40</b>	<b>50.22</b>	70.07	11.16	39.33	58.67	11.44	29.48	80.00	8.70	37.69	63.44	9.61	32.91	74.24	12.58	30.15
Speech LSNN																		
Mismatch	Forward Noise + Beta 0.5			Beta 0.5			Standard			Forward Noise			AWP			Dropout = 0.3		
	Mean Acc.	Std.	Min.	Mean Acc.	Std.	Min.	Mean Acc.	Std.	Min.	Mean Acc.	Std.	Min.	Mean Acc.	Std.	Min.	Mean Acc.	Std.	Min.
0.0	81.52	0.05	81.47	<b>82.48</b>	<b>0.00</b>	<b>82.48</b>	80.86	0.03	80.83	81.33	0.14	81.20	81.35	0.12	81.23	79.02	0.36	78.66
0.1	81.33	<b>0.24</b>	80.72	<b>82.01</b>	0.31	<b>81.03</b>	79.72	0.45	78.53	81.12	0.32	80.18	80.85	0.38	79.71	79.16	0.44	77.88
0.2	80.77	<b>0.35</b>	79.71	<b>81.24</b>	0.43	<b>79.98</b>	76.96	1.11	72.57	80.10	0.53	78.73	79.24	0.66	77.54	78.58	0.67	75.85
0.3	79.57	<b>0.62</b>	<b>77.98</b>	<b>79.80</b>	0.67	77.54	72.31	2.00	65.40	78.05	0.88	75.45	76.35	1.23	70.04	77.18	0.96	74.83
0.5	72.67	2.75	<b>63.85</b>	<b>73.40</b>	<b>2.32</b>	60.91	57.16	4.25	42.07	67.41	3.93	53.50	63.50	4.18	45.92	69.80	3.13	54.75
0.7	58.03	6.57	32.19	<b>60.23</b>	<b>4.66</b>	<b>45.49</b>	40.70	5.72	24.92	49.19	6.98	30.47	45.96	5.61	22.56	55.96	5.74	37.74

attacks in the full network parameter space, increasing the robustness of spiking networks. The technique of interval bound propagation can also be applied to these additional network parameters.

We did not quantize network parameters either during or after training, in this work. This quantization step, ideally performed during training, is required to deploy networks to specialized neuromorphic inference hardware. It is not obvious how our adversarial attacks would interact with quantization during the training process.

We believe there is a connection between our regularisation and minimal description length, due to the fact that robust parameters can be encoded with less precision. This can be seen using a bits back argument as described in [41]. Further analysis is needed to explore this connection.

**Broader impact** Our work can be considered an enabling technology for ultra-low-power edge computation, based on mixed-signal neuromorphic processors and AI processors using memristor cross-bar arrays. Ultra-low-power edge inference has several ethical implications, both positive and negative. Edge inference technologies can be inherently privacy preserving, since recording and sharing of personally-identifiable data such as audio and video streams is no longer needed. By processing data locally, personal data can be kept off insecure networks and can be protected from undesired databasing in the cloud. On the other hand, ultra low-power operation makes it more feasible to implement always-on monitoring in edge devices. This raises all the same ethical issues as surveillance technology in general, with the additional concern that edge surveillance devices can be made more surreptitious, and with longer battery life.

Our method improves the performance of neural networks deployed to inference hardware that include computational non-idealities. For example, NN processors with crossbar architectures based on novel memory devices such as RRAM and PCM memristors [4] display uncertainty in stored memory values as well as value drift over time [5–7]. Analog neurons and synapses in mixed-signal NN processors, for example SNN inference processors [9], exhibit variation in weights and neuron parameters across a processor.

We showed that our training approach finds network solutions that are insensitive to mismatch-induced parameter variation. Our networks can therefore be deployed to inference devices with computational non-idealities with only minimal reduction in task performance, and without requiring per-device calibration or model training. This reduction in per-device handling implies a considerable reduction in expense when deploying at commercial scale. Our method therefore brings low-power neuromorphic inference processors closer to commercial viability.

## Acknowledgments and Disclosure of Funding

This work was partially supported by EU grants 826655 “TEMPO”; 871371 “MEMSCALES”; and 876925 “ANDANTE” to DRM.

## References

- [1] Huang, S., Xiao, S. & Feng, W. On the energy efficiency of graphics processing units for scientific computing. In *2009 IEEE International Symposium on Parallel Distributed Processing*, 1–8 (2009).
- [2] Chen, A. A review of emerging non-volatile memory (nvm) technologies and applications. *Solid-State Electronics* **125**, 25–38 (2016). URL <https://www.sciencedirect.com/science/article/pii/S0038110116300867>. Extended papers selected from ESSDERC 2015.
- [3] Yu, S. & Chen, P.-Y. Emerging memory technologies: Recent trends and prospects. *IEEE Solid-State Circuits Magazine* **8**, 43–56 (2016).
- [4] Verma, N. *et al.* In-memory computing: Advances and prospects. *IEEE Solid-State Circuits Magazine* **11**, 43–55 (2019).
- [5] Le Gallo, M. *et al.* Mixed-precision in-memory computing. *Nature Electronics* **1**, 246–253 (2018). URL <https://doi.org/10.1038/s41928-018-0054-8>.
- [6] Wu, L., Liu, H., Li, J., Wang, S. & Wang, X. A Multi-level Memristor Based on Al-Doped HfO<sub>2</sub> Thin Film. *Nanoscale Research Letters* **14**, 177 (2019). URL <https://doi.org/10.1186/s11671-019-3015-x>.
- [7] Joshi, V. *et al.* Accurate deep neural network inference using computational phase-change memory. *Nature Communications* **11**, 2473 (2020). URL <https://doi.org/10.1038/s41467-020-16108-9>.
- [8] Neckar, A. *et al.* Braindrop: A mixed-signal neuromorphic architecture with a dynamical systems-based programming model. *Proceedings of the IEEE* **107**, 144–164 (2019).
- [9] Moradi, S., Qiao, N., Stefanini, F. & Indiveri, G. A scalable multicore architecture with heterogeneous memory structures for dynamic neuromorphic asynchronous processors (dynaps). *IEEE Transactions on Biomedical Circuits and Systems* **12**, 106–122 (2018).
- [10] Cassidy, A. S. *et al.* Truenorth: A high-performance, low-power neurosynaptic processor for multi-sensory perception, action, and cognition (2016).
- [11] Schemmel, J. *et al.* A wafer-scale neuromorphic hardware system for large-scale neural modeling. In *2010 IEEE International Symposium on Circuits and Systems (ISCAS)*, 1947–1950 (2010).
- [12] Ambrogio, S. *et al.* Equivalent-accuracy accelerated neural-network training using analogue memory. *Nature* **558**, 60–67 (2018). URL <https://doi.org/10.1038/s41586-018-0180-5>.
- [13] Bauer, F. C., Muir, D. R. & Indiveri, G. Real-time ultra-low power ecg anomaly detection using an event-driven neuromorphic processor. *IEEE Transactions on Biomedical Circuits and Systems* **13**, 1575–1582 (2019).
- [14] Nandakumar, S. R. *et al.* Mixed-precision deep learning based on computational memory. *Frontiers in Neuroscience* **14**, 406 (2020). URL <https://www.frontiersin.org/article/10.3389/fnins.2020.00406>.
- [15] Thakur, C. S. *et al.* An analogue neuromorphic co-processor that utilizes device mismatch for learning applications. *IEEE Transactions on Circuits and Systems I: Regular Papers* **65**, 1174–1184 (2018).
- [16] Büchel, J., Zendrikov, D., Solinas, S., Indiveri, G. & Muir, D. R. Supervised training of spiking neural networks for robust deployment on mixed-signal neuromorphic processors (2021). [2102.06408](https://arxiv.org/abs/2102.06408).
- [17] Srivastava, N., Hinton, G., Krizhevsky, A., Sutskever, I. & Salakhutdinov, R. Dropout: A simple way to prevent neural networks from overfitting. *Journal of Machine Learning Research* **15**, 1929–1958 (2014). URL <http://jmlr.org/papers/v15/srivastava14a.html>.
- [18] Murray, A. & Edwards, P. Enhanced mlp performance and fault tolerance resulting from synaptic weight noise during training. *IEEE Transactions on Neural Networks* **5**, 792–802 (1994).
- [19] Wang, Y. *et al.* Improving adversarial robustness requires revisiting misclassified examples. In *International Conference on Learning Representations* (2020). URL <https://openreview.net/forum?id=rk10g6EFwS>.

- [20] Zhang, H. *et al.* Theoretically principled trade-off between robustness and accuracy. *CoRR abs/1901.08573* (2019). URL <http://arxiv.org/abs/1901.08573>. 1901.08573.
- [21] Madry, A., Makelov, A., Schmidt, L., Tsipras, D. & Vladu, A. Towards deep learning models resistant to adversarial attacks (2019). 1706.06083.
- [22] Moosavi-Dezfooli, S., Fawzi, A., Uesato, J. & Frossard, P. Robustness via curvature regularization, and vice versa. *CoRR abs/1811.09716* (2018). URL <http://arxiv.org/abs/1811.09716>. 1811.09716.
- [23] Cicek, S. & Soatto, S. Input and weight space smoothing for semi-supervised learning. In *2019 IEEE/CVF International Conference on Computer Vision Workshop (ICCVW)*, 1344–1353 (2019).
- [24] Wu, D., Wang, Y. & Xia, S. Revisiting loss landscape for adversarial robustness. *CoRR abs/2004.05884* (2020). URL <https://arxiv.org/abs/2004.05884>. 2004.05884.
- [25] Chaudhari, P. *et al.* Entropy-SGD: biasing gradient descent into wide valleys. *Journal of Statistical Mechanics: Theory and Experiment* **2019**, 124018 (2019). URL <https://doi.org/10.1088%2F1742-5468%2F1901/124018>.
- [26] Carlini, N. & Wagner, D. A. Towards evaluating the robustness of neural networks. *CoRR abs/1608.04644* (2016). URL <http://arxiv.org/abs/1608.04644>. 1608.04644.
- [27] Moosavi-Dezfooli, S., Fawzi, A. & Frossard, P. Deepfool: a simple and accurate method to fool deep neural networks. *CoRR abs/1511.04599* (2015). URL <http://arxiv.org/abs/1511.04599>.
- [28] Goodfellow, I. J., Shlens, J. & Szegedy, C. Explaining and harnessing adversarial examples (2015). 1412.6572.
- [29] Li, H., Xu, Z., Taylor, G., Studer, C. & Goldstein, T. Visualizing the loss landscape of neural nets. In Bengio, S. *et al.* (eds.) *Advances in Neural Information Processing Systems*, vol. 31 (Curran Associates, Inc., 2018). URL <https://proceedings.neurips.cc/paper/2018/file/a41b3bb3e6b050b6c9067c67f663b915-Paper.pdf>.
- [30] Gabay, D. & Mercier, B. A dual algorithm for the solution of nonlinear variational problems via finite element approximation. *Computers & Mathematics with Applications* **2**, 17–40 (1976). URL <https://www.sciencedirect.com/science/article/pii/0898122176900031>.
- [31] Dai, Y.-H. Fast algorithms for projection on an ellipsoid. *SIAM Journal on Optimization* **16**, 986–1006 (2006). URL <https://doi.org/10.1137/040613305>. <https://doi.org/10.1137/040613305>.
- [32] Cho, M. *et al.* 17.2 a 142nm voice and acoustic activity detection chip for mm-scale sensor nodes using time-interleaved mixer-based frequency scanning. In *2019 IEEE International Solid-State Circuits Conference - (ISSCC)*, 278–280 (2019).
- [33] Gies, V., Marzetti, S., Barchasz, V., Barthélemy, H. & Glotin, H. Ultra-low power embedded unsupervised learning smart sensor for industrial fault classificatio. In *2020 IEEE International Conference on Internet of Things and Intelligence System (IoT&IS)*, 181–187 (2021).
- [34] Liu, Q. *et al.* Live demonstration: Face recognition on an ultra-low power event-driven convolutional neural network asic. In *2019 IEEE/CVF Conference on Computer Vision and Pattern Recognition Workshops (CVPRW)*, 1680–1681 (2019).
- [35] Warden, P. Speech Commands: A Dataset for Limited-Vocabulary Speech Recognition. *ArXiv e-prints* (2018). URL <https://arxiv.org/abs/1804.03209>. 1804.03209.
- [36] Xiao, H., Rasul, K. & Vollgraf, R. Fashion-mnist: a novel image dataset for benchmarking machine learning algorithms (2017). 1708.07747.
- [37] Kingma, D. P. & Ba, J. Adam: A method for stochastic optimization. In Bengio, Y. & LeCun, Y. (eds.) *3rd International Conference on Learning Representations, ICLR 2015, San Diego, CA, USA, May 7-9, 2015, Conference Track Proceedings* (2015). URL <http://arxiv.org/abs/1412.6980>.
- [38] Cousot, P. & Cousot, R. Abstract interpretation: A unified lattice model for static analysis of programs by construction or approximation of fixpoints. In *Proceedings of the 4th ACM SIGACT-SIGPLAN Symposium on Principles of Programming Languages, POPL '77*, 238–252 (Association for Computing Machinery, New York, NY, USA, 1977). URL <https://doi.org/10.1145/512950.512973>.

- [39] Gehr, T. *et al.* Ai2: Safety and robustness certification of neural networks with abstract interpretation. In *2018 IEEE Symposium on Security and Privacy (SP)*, 3–18 (2018).
- [40] Mirman, M., Gehr, T. & Vechev, M. T. Differentiable abstract interpretation for provably robust neural networks. In Dy, J. G. & Krause, A. (eds.) *Proceedings of the 35th International Conference on Machine Learning, ICML 2018, Stockholmsmässan, Stockholm, Sweden, July 10-15, 2018*, vol. 80 of *Proceedings of Machine Learning Research*, 3575–3583 (PMLR, 2018). URL <http://proceedings.mlr.press/v80/mirman18b.html>.
- [41] Honkela, A. & Valpola, H. Variational learning and bits-back coding: an information-theoretic view to bayesian learning. *IEEE Transactions on Neural Networks* **15**, 800–810 (2004).
- [42] Bellec, G., Salaj, D., Subramoney, A., Legenstein, R. A. & Maass, W. Long short-term memory and learning-to-learn in networks of spiking neurons. *CoRR* **abs/1803.09574** (2018). URL <http://arxiv.org/abs/1803.09574>. 1803.09574.
- [43] Glorot, X. & Bengio, Y. Understanding the difficulty of training deep feedforward neural networks. In Teh, Y. W. & Titterton, M. (eds.) *Proceedings of the Thirteenth International Conference on Artificial Intelligence and Statistics*, vol. 9 of *Proceedings of Machine Learning Research*, 249–256 (JMLR Workshop and Conference Proceedings, Chia Laguna Resort, Sardinia, Italy, 2010). URL <http://proceedings.mlr.press/v9/glorot10a.html>.

## Supplementary Material

### Architectures

#### Spiking RNN Architecture

The dynamics of the spiking model [42] can be summarised by a set of differential equations (Eq. 3).

$$\begin{aligned}
 \mathbf{B}^t &= \mathbf{b}^0 + \beta \mathbf{b}^t \\
 \mathbf{o}^t &= \mathbf{1}(\mathbf{V}^t > \mathbf{B}^t) \text{ unless refractory } t_{\text{refr}} \\
 \mathbf{b}^{t+1} &= \rho_\beta \mathbf{b}^t + (1 - \rho_\beta) \frac{\mathbf{o}^t}{dt} \\
 \mathbf{I}_{\text{Reset}}^t &= \frac{\mathbf{o}^t}{dt} \mathbf{B}^t dt \\
 \mathbf{V}^{t+1} &= \rho_V \mathbf{V}^t + (1 - \rho_V)(\mathbf{I}_{\text{in}} W_{\text{in}} + \frac{\mathbf{o}^t}{dt} W_{\text{rec}}) - \mathbf{I}_{\text{Reset}}^t
 \end{aligned} \tag{3}$$

where  $\rho_\beta = e^{-dt/\tau_{\text{ada}}}$  and  $\rho_V = e^{-dt/\tau}$ . The variables  $\mathbf{B}$  describe the spiking thresholds with spike-frequency adaptation. The vector  $\mathbf{o}^t$  denotes the population spike train at time  $t$ . The membrane potentials  $\mathbf{V}$  have a time constant  $\tau$  and the adaptive threshold time constant is denoted by  $\tau_{\text{ada}}$ . The speech signals and ECG traces fed into the network are represented as currents  $\mathbf{I}_{\text{in}}$ . Since the derivative of the spiking function with respect to its input is mostly 0 we use a surrogate gradient that is explicitly defined as

$$\frac{\partial E}{\partial \mathbf{V}^t} = \frac{\partial E}{\partial \mathbf{z}^t} \frac{\partial \mathbf{z}^t}{\partial \mathbf{V}^t} = \frac{\partial E}{\partial \mathbf{z}^t} d \cdot \max\left(\mathbf{1} - \left| \frac{\mathbf{V}^t - \mathbf{B}^t}{\mathbf{B}^t} \right|, \mathbf{0}\right) \tag{4}$$

where  $E$  is the error and  $d$  is the dampening factor. To get the final prediction of the network, we average the population spike trains along the time-axis  $\mathbf{z}_{\text{avg}}$  and compute

$$\begin{aligned}
 \mathbf{l} &= \text{softmax}(\mathbf{z}_{\text{avg}} W_{\text{out}} + \mathbf{b}_{\text{out}}) \\
 \hat{y} &= \underset{i}{\text{argmax}} \mathbf{l}_i
 \end{aligned}$$

#### CNN Architecture

Our architecture comprises two convolutional blocks ( $2 \times [4 \times 4, 64 \text{ channels, MaxPool, ReLU}]$ ), followed by three dense layers ( $N = 1600, 256, 64, \text{ReLU}$ ) and a softmax layer. All weights and kernels are initialized using the Glorot normal initialisation [43]. Using this architecture, we achieved a test accuracy of  $\sim 93\%$ . Attacked parameters for this network included all the kernel weights, as well as all the dense layer parameters.

#### Derivation of Jacobian

Under the assumption that  $\alpha = \frac{\zeta \odot |\Theta|}{N_{\text{steps}}}$  and  $p = \infty$ , we can rewrite the inner loop of Algorithm 1 to

```

begin
   $\Theta^* \leftarrow \Theta + |\Theta| \epsilon \odot R ; R \sim \mathcal{N}(0, 1)$ 
  for  $t = 1$  to  $N_{\text{steps}}$  do
     $\Theta_t^* \leftarrow \Theta_{t-1}^* + \alpha \cdot \text{sign} \left( \nabla_{\Theta_{t-1}^*} \mathcal{L}_{\text{Rob}}(f(\Theta, X), f(\Theta_{t-1}^*, X)) \right)$ 
  end
end

```

By rewriting  $\Theta^*$  in the form of  $\Theta^* = \Theta + \Delta\Theta$  we get

$$\Theta^* = \Theta + |\Theta| \epsilon \odot R + \alpha \odot \sum_{t=1}^{N_{\text{steps}}} \text{sign} \left( \nabla_{\Theta_{t-1}^*} \mathcal{L}_{\text{Rob}}(f(\Theta, X), f(\Theta_{t-1}^*, X)) \right)$$

From this the Jacobian can be easily calculated. Plugging in the definition for  $\alpha$  we get

$$\mathbf{J}_{\Theta^*}(\Theta) = \mathbf{I} + \text{diag} \left[ \frac{\text{sign}(\Theta) \odot (\zeta + \epsilon \cdot R_1)}{N_{\text{steps}}} \odot \sum_{t=1}^{N_{\text{steps}}} \text{sign}(\nabla_{\Theta_t^*} \mathcal{L}_{\text{Rob}}(f(\Theta, X), f(\Theta_t^*, X))) \right]$$

### Weight loss-landscape visualization

We characterized the shape of the weight loss-landscape by plotting the categorical cross entropy loss for varying levels of noise added to the weights of the trained network. In each trial, we picked a random vector  $v \sim \mathcal{N}(\mathbf{0}, \zeta|\Theta|)$  and evaluated the categorical cross entropy of the whole test set given the weights  $\Theta + \alpha \cdot v$ , where  $\alpha \in [-2, 2]$  and  $\zeta = 0.2$ . As we show in Figure S1, the variance of the individual 1D weight loss-landscapes is small.

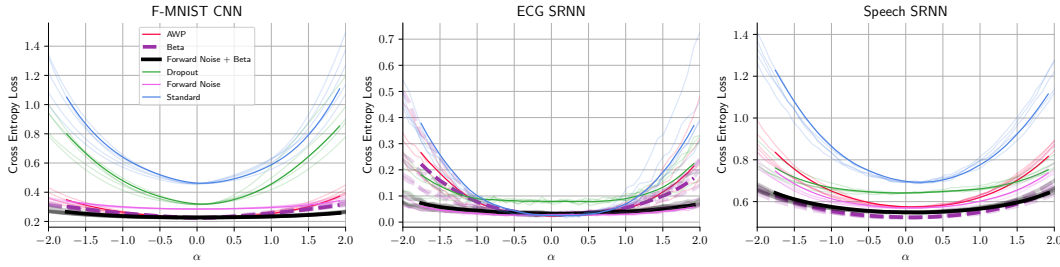


Figure S1: Illustration of the 1D weight loss-landscape including the individual trials.

### Additional Results

While the adversary in AWP approximates  $\max \mathcal{L}_{\text{cat. cross-entropy}}(f(\Theta^*, X), y)$ , the adversary in our algorithm approximates  $\max \text{KL}(f(\Theta, X), f(\Theta^*, X))$ . In the experiment section we evaluate the robustness of the various methods to an adversary attacking the cross-entropy loss in order to not give our method an unfair advantage since it was trained using an adversary that maximizes the KL-divergence. Figure S2 shows the adversarial robustness of the methods for an adversary that attacks the KL-divergence rather than the cross-entropy loss.

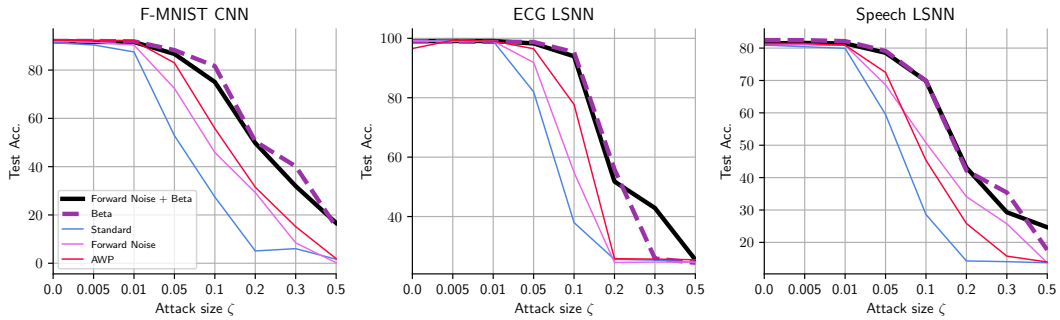


Figure S2: Adversarial robustness for adversary that aims at maximizing the KL-divergence between the normal and attacked network.

Figure S3 illustrates the test accuracy of two MLPs trained on F-MNIST over the course of training. Using an inverse weight decay term, the weight-magnitude of one network is forced to 2.0 (black cross), while the other networks weight magnitude (red cross) remains stable. One can observe that as the weight magnitude of the one network increases, also the robustness to Gaussian noise ( $\epsilon = 0.2$ ) increases (blue), while the performance of the other network remains poor (cyan).

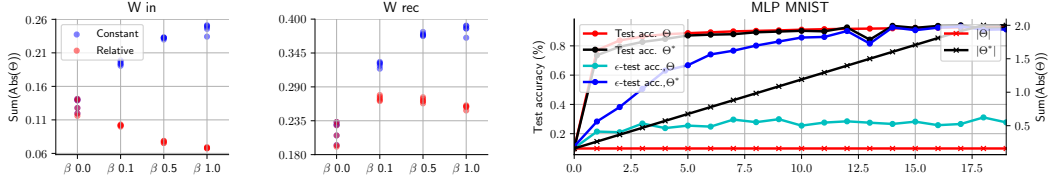


Figure S3: (left,middle) When the adversary is limited to a constant, parameter-independent perturbation, trivial solutions occur by scaling up the parameters (blue). If the space in which the adversary can search for a perturbation depends linearly on the weight magnitude, non-trivial solutions must be found. (right) Training an MLP on F-MNIST using inverse weight decay to increase the robustness ( $\epsilon$ -test acc.) against noise with constant magnitude.

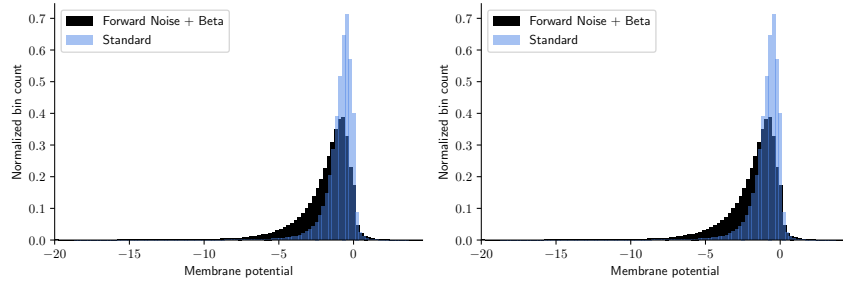


Figure S4: **Membrane potentials are distributed away from the firing threshold for networks trained with forward noise.** We measured the distribution of membrane potentials in SRNNs trained using standard gradient descent (“Standard”), and in the presence of weight noise injected in the forward pass (“Robust”). As predicted, networks trained with forward noise have membrane potentials distributed away from the firing threshold. This implies that weight perturbations are less likely to inject or delete a spike erroneously, improving the robustness of the network.

### Wide-margin network activations

Murray et al. show that adding random forward noise to the weights of a network during the forward pass implicitly adds a regularizer of the form  $\Theta_{ij}^2 \left( \frac{\partial o_{kl}}{\partial \Theta_{ij}} \right)^2$  to the network weights [18]. When sigmoid activation functions are used, this regularizer favors high or low activations. When implementing interval bound propagation for SRNNs, intervals over spiking activity must be computed by passing intervals through the spiking threshold function. As a result, intervals for spiking activity become either  $[0, 0]$  for neurons that never emit a spike regardless of weight attack;  $[1, 1]$  for neurons that always emit a spike; and  $[0, 1]$  for neurons for which activity becomes uncertain in the presence of weight attack. By definition, a robust network should promote bounds  $[0, 0]$  and  $[1, 1]$ , where the activity of the network is unchanged by weight attack. Robust network configurations should therefore avoid states where the membrane potentials of neurons are close to the firing threshold.

To see whether this was also the case for our SRNNs, we investigated the distribution of the membrane potentials on a batch of test examples for a network that was trained with- and without noise during the forward pass. We found that robust networks exhibited a broader distribution of membrane potentials, with comparatively less distribution mass close to the firing threshold (Fig. S4). This indicates that neurons in the robust network spend more time in a “safe” regime where a small change in the weights cannot trigger an unwanted spike, or remove a desired spike.